

On the Viewing Angle Dependence of Blazar Variability

Avigdor Eldar and Amir Levinson

School of Physics and Astronomy, Tel Aviv University, Tel Aviv 69978, Israel

Accepted Received in original form 21 November 2018

ABSTRACT

Internal shocks propagating through an ambient radiation field, are subject to a radiative drag that, under certain conditions, can significantly affect their dynamics and, consequently, the evolution of the beaming cone of emission produced behind the shocks. The resultant change of the Doppler factor combined with opacity effects leads to a strong dependence of the variability pattern produced by such systems, specifically, the shape of the light curves and the characteristics of correlated emission, on viewing angle. One implication is that objects oriented at relatively large viewing angles to the observer should exhibit a higher level of activity at high synchrotron frequencies (above the self-absorption frequency) and at gamma-ray energies below the threshold energy to pair production, than at lower (radio/millimeter) frequencies.

Key words: galaxies:jets - radiation mechanisms:nonthermal - relativity

1 INTRODUCTION

The rapid variability often exhibited by blazars and GRBs is widely attributed to formation of internal shocks in the expelled outflow (see e.g., Rees 1978; Romanova & Lovelace 1997; Levinson 1998, in the context of blazars, and Rees & Meszaros, 1994; Eichler 1994; Sari & Piran 1997, in the context of GRBs). Internal shocks are produced as a result of unsteadiness of the source, which ultimately leads to overtaking collisions of different fluid slabs. The observed variability time associated with a single front is on the order of the light travel time across the expelled fluid slab (provided the cooling time is sufficiently short, and that the slab is optically thin and not too thick geometrically), and, therefore, can be as short as the intrinsic timescale (e.g., the dynamical time of the central engine). If indeed associated with the gravitational radius of the putative black hole, this timescale comes out to be of order milliseconds in the case of GRBs, and minutes to hours in the case of blazars, consistent with the temporal substructure seen in these two classes of objects (e.g., Wagner, 1997; Ulrich, et al., 1997; Fishman & Meegan, 1995). The fraction of bulk energy that can be dissipated behind the shocks and, provided the cooling time is sufficiently short, radiated away, depends mainly on the difference in Lorentz factors of the colliding shells. In scenarios that invoke magnetically dominated outflows, effective dissipation of the shocked magnetic field is also required for high radiative efficiency (e.g., Levinson & Van Putten 1997).

The dynamics of internal fronts and the resulting variability pattern depend on the parameters of the expelled fluid and on environmental conditions. In particular, in situations whereby the front moves through an intense, roughly isotropic (in the frame of the central engine) radiation field,

as in ERC models, it will be subject to a radiative drag that can affect its dynamics and emission considerably. In the model considered here (see, Levinson, 1998 [Paper I]; Levinson 1999a [Paper II] for details), the created front is assumed to be adiabatic initially. During the adiabatic phase, shortly after its creation and prior to the onset of radiative losses, the front moves at some constant velocity intermediate between that of the colliding fluid slabs, such that the net momentum flux incident through the shocks and, consequently, the net force exerted on the front by the “push” of the exterior fluids vanish. A fraction of the energy dissipated behind the shocks is tapped for the acceleration of electrons to nonthermal energies and the rest to heat the front. The injected electrons then cool adiabatically, owing to the front expansion, and radiatively through synchrotron emission and inverse Compton scattering of external, soft photons (ERC emission). Since the synchrotron emission is isotropic in the comoving frame it does not contribute to momentum losses. However, the ERC emission, which is highly beamed in the front frame, gives rise to a radiative drag that leads to deceleration of the front during the rise of the emitted ERC power. The increasing radiative friction is balanced by an excess momentum transfer to the front from the fluid behind it (the fast fluid). The reason is that as the front decelerates the relative velocity between the front and the fast fluid and, hence, the net momentum flux incident through the reverse shock increases, while the net momentum flux incident through the forward shock decreases. The decelerating front will reach its minimum Lorentz factor roughly when the total ERC power radiated by the front peaks, provided the shock crossing time of the expelled fluid slabs is sufficiently long. If the intensity of external radia-

tion declines with radius, as envisaged here, then the ERC flux radiated by the front and the associated drag will decline as the front moves outwards. This would then lead to re-acceleration of the front, following peak emission, until its initial speed and structure are restored (or until shock crossing of the fluid slabs is completed). The external, soft photons also contribute a large pair production opacity that can lead to absorption of escaping gamma rays and the initiation of pair cascades inside and ahead of the front at early times. This, in turn, will affect the evolution of the high energy spectrum. The synchrotron opacity also changes with time, owing to the front expansion. We stress that the variability in this model reflects the dynamics of the front and the radial profiles of the magnetic field and external photon intensity, and is not due to any explicit time changes of the front parameters or particle injection. To be concrete, in the case of long outbursts the variability is caused by a change in the Thomson and synchrotron opacities during the course of the front that result from the radial variations of external photon intensity and magnetic field. In the case of short outbursts the variability is due to shock crossing (after which energy deposition in the front ceases) and the subsequent cooling of the hot fluid slabs. The combination of time varying Lorentz factor and optical depth effects should give rise to a certain dependence of the variability pattern on the viewing angle (Levinson 1999b). It is the purpose of this paper to explore this orientation effect within the framework of the radiative front model developed in Papers I and II.

2 INTENSITY AND OBSERVED FLUX

In Papers I and II we analyzed the structure and dynamics of a radiative front and computed the temporal evolution of the angle averaged flux radiated during its course. In this section we generalize our previous treatment to allow for the calculation of the angular dependence of the emission. The structure and dynamics of the front are computed as before using the model developed in Paper I, but the equations governing the evolution of the radiated flux have been modified in a manner described below. The model assumes that a constant fraction of the power dissipated behind the shocks is injected in the form of nonthermal electron distribution. The rate of energy dissipation inside the front depends, in turn, on the relative velocities between the exterior fluids and the front and is computed self consistently. The electron acceleration time is assumed to be much shorter than the cooling and light crossing times, so that it does not affect the evolution of the radiated ERC and synchrotron spectra. The energy distributions of electrons, gamma-rays and synchrotron photons inside the front are computed by solving the appropriate kinetic equations, which are coupled to the MHD equations governing the front dynamics through the injection term and the energy and momentum loss terms. As shown in Papers I and II, the energy distribution of emitting electrons is determined essentially by the pair cascade and cooling processes and is insensitive to the form of injected electron spectrum, provided the acceleration process is efficient and that the Thomson opacity contributed by the external radiation field is large enough. In the examples presented below the injected spectrum was taken to be a power law with roughly equal energy injection rate per log energy.

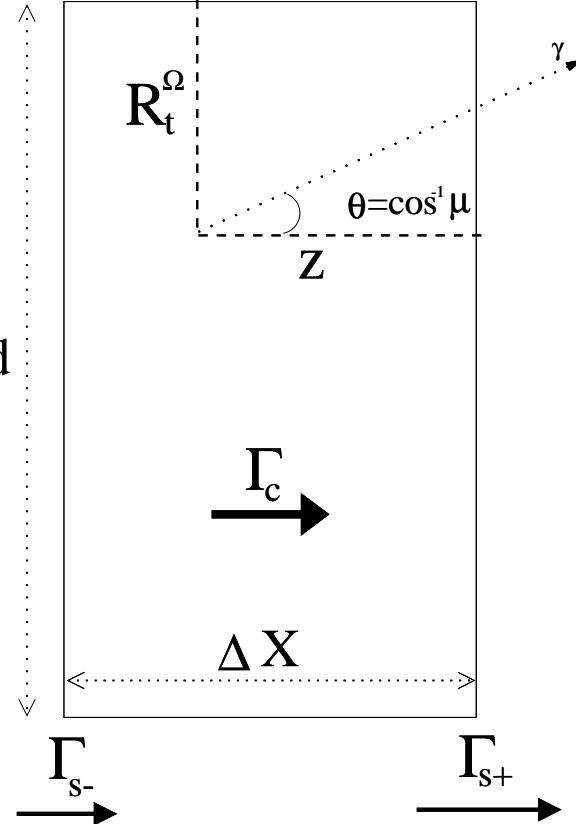


Figure 1. Schematic illustration of the front structure.

We approximate the front (see fig. 1) as a cylindrical section with an axial length ΔX and cross sectional radius d , and denote by β_c , β_{s+} and β_{s-} the velocity of the front, the forward and reverse shocks with respect to the injection frame, respectively, and by Γ_c , $\Gamma_{s\pm}$ the corresponding Lorentz factors. We suppose that in addition to its radial expansion, which is computed from the model, the front expands also sideways at some velocity, taken to be a fraction $\psi \ll 1$ of β_c . This then yields $d(t) = \psi r(t)$, where $r(t) = r_o + c \int \beta_c dt$ is the position of the front (more precisely, the contact discontinuity) at time t . We stress that the shock geometry invoked here is probably unrealistic, since the perimeter of the forward shock moves at velocity $\beta_c \sqrt{1 + \psi^2}$ that may violate causality under certain choice of parameters. The shock is more likely to be curved, or even corrugated as a result of instabilities. We do not expect, however, our results to be strongly dependent upon shock geometry, but merely on the characteristic velocities. We further assume that the electron distribution is isotropic and homogeneous inside the front, and denote by $j_\nu(\mu, t)$ and $\kappa_\nu(\mu, t)$ the emission and absorption coefficients of some radiation process (e.g., synchrotron or ERC emission), as measured in the injection frame. In the case of synchrotron emission, the latter assumption implies that j_ν and κ_ν are also isotropic and homogeneous inside the front (but not necessarily the intensity). This is not true, however, for the ERC emission (Dermer, 1995), since the comoving distribution of scattered photons is highly anisotropic.

Consider now a photon emitted at time t at some position inside the front in the direction $\hat{\Omega}$, and denote by z_t the

distance between the location from which the photon is emitted and the forward shock, and by R_t^Ω the distance along the projection of $\hat{\Omega}$ on the plane perpendicular to the front axis (that is, along the vector $\hat{\Omega} - \mu\hat{z}$, where $\mu = \hat{\Omega} \cdot \hat{z}$) between the emission point and the front boundary (see fig. 1). Now, the photon (if not absorbed) will escape from the front through the forward shock if $c\bar{t} \sin \theta < R_t^\Omega$ (ignoring the transverse expansion of the front), and through the sides when the opposite inequality holds. Here $\sin \theta = \sqrt{1 - \mu^2}$, and \bar{t} is given implicitly by $\bar{t} = (z_t/c + \int^{\bar{t}} \beta_{s+} dt)/\mu$. In terms of the time averaged shock velocity, $\bar{\beta}_{s+}$, one obtains, $c\bar{t} = z_t/(\mu - \bar{\beta}_{s+})$, so that the condition that the photon will escape through the forward shock reads: $z_t < R_t^\Omega(\mu - \bar{\beta}_{s+})/\sin \theta$. Note that photons emitted into directions $\mu < \bar{\beta}_{s+}$ can only escape from the sides.

The intensity crossing the front boundary along the direction $\hat{\Omega}$, at some position Σ on the boundary surface, is given, under the above assumptions, by

$$I_\nu(\Sigma, \hat{\Omega}, t) = \int_0^{t_\Sigma} j_\nu(\hat{\Omega}, t - \chi) e^{-\tau_\nu(\chi)} c d\chi, \quad (1)$$

where $\tau_\nu(\chi) = c \int_0^\chi \kappa_\nu(\chi') d\chi'$ is the optical depth traversed by a photon emitted at time $t - \chi$, and t_Σ is the light crossing time of the expanding front along the corresponding ray, measured in the frame of the central engine. The flux emitted from the boundary surface at some location is given by $I_\nu(\Sigma, \hat{\Omega}, t)(\hat{\Omega} \cdot \hat{n} - \hat{\beta}_\Sigma \cdot \hat{n})$, where \hat{n} is the normal to the surface, and β_Σ is the velocity of the surface at the corresponding position (for instance $\beta_\Sigma = \beta_{s+}\hat{z}$ for any point on the forward shock surface). This must be multiplied by the time dilation factor, $(1 - \beta_\Sigma \cdot \hat{\Omega})^{-1}$, in order to obtain the observed flux. One finds,

$$\mathcal{F}_\nu = \frac{(1+Z)}{D_L^2} \int_\Sigma I_\nu(\Sigma, \hat{\Omega}, t) \frac{(\hat{\Omega} \cdot \hat{n} - \hat{\beta}_\Sigma \cdot \hat{n})}{1 - \beta_\Sigma \cdot \hat{\Omega}} d\Sigma. \quad (2)$$

Here D_L is the luminosity distance and Z is the corresponding redshift. We note that the time evolution of β_Σ and the remaining front parameters is computed using the front equations derived in Paper I. It is also worth-noting that the observed time change, $t_{obs} = \int (1 - \beta_\Sigma \cdot \hat{\Omega}) dt$, may be different for different emitting surfaces, so that the observed time structure may reflect, to some extent, the geometry of the front. The above treatment modifies the analysis presented in Papers I and II to account for retardation effects associated with the front expansion and with rapid time changes of the emissivity and opacity. We find that this modification does not give rise to significant alterations of the results obtained in Papers I and II for the evolution of the angle averaged flux, but does improve slightly the calculations of the light curves observed at relatively large viewing angles.

As a simple example consider a non-expanding blob moving with a velocity β_c , and let the volume emissivity be time independent. Then $\beta_\Sigma = \beta_c\hat{z}$, and equations (1) and (2) yield for the optically thin flux, $\mathcal{F}_\nu \propto \frac{j_\nu V}{(1 - \beta_c \mu)}$, where $V = ct_\Sigma \int d\Sigma$ is the volume of the front. In terms of the comoving volume, $V' = \Gamma_c V$, and comoving emissivity, the observed flux reduces to the familiar expression: $\mathcal{F}_\nu = \frac{(1+Z)}{D_L^2} \mathcal{D}_c^3 j'_\nu V'$, with $\mathcal{D}_c = [\Gamma_c(1 - \beta_c \mu)]^{-1}$ being the corresponding Doppler factor. As a second example, consider the flux emitted from an expanding, stationary front in the forward direction, viz., $\mu = 1$. In that case the entire flux is

emitted through the forward shock. The corresponding time dilation factor is then $(1 - \beta_{s+})^{-1}$, and the light crossing time along the front's axis is $t_\Sigma = \bar{t} = \Delta X/(1 - \beta_{s+})$. From equations (1) and (2) we obtain, again in the optically thin limit,

$$\mathcal{F}_\nu = \frac{(1+Z)}{D_L^2} \mathcal{D}_{s+} \mathcal{D}_c^2 (\Gamma_{s+}/\Gamma_c) V' j'_\nu,$$

with \mathcal{D}_{s+} being the Doppler factor associated with the forward shock. This example illustrates the effect of the expansion on the emitted flux. The enhancement of the forward flux by a factor $(\Gamma_{s+}/\Gamma_c)^2$ is entirely due the growth of the front's volume.

The integration of eq. (1) for a specific process requires the determination of the corresponding volume emissivity j_ν . The determination of the synchrotron emissivity is straightforward, since the emission is isotropic in the front frame, and is described in Paper II. The ERC emissivity is calculated using the head-on approximation; that is, the direction of scattered photon is taken to be along the direction of the scattering electron. The electron distribution in the injection frame, denoted by $n_e(E_e, \mu, t)$, is obtained at each time step by appropriate Lorentz transformation of the comoving electron distribution which, as mentioned above, assumed to be isotropic. Using this approximations the ERC emissivity can be expressed as,

$$j_{ERC}(E_\gamma, \mu, t) = \int n_e(E_e, \mu, t) \eta_{c\gamma}(E_\gamma, E_e, t) dE_e \quad (3)$$

where $\eta_{c\gamma}$ is the corresponding redistribution function, and is given explicitly in Blandford & Levinson (1995). Note that η is independent of μ by virtue of the assumed isotropy of the ambient radiation field. Finally, since we consider only cases for which gamma-ray production is dominated by ERC emission, we neglect the SSC emissivity in eq. (1) (see §4 for further discussion).

3 RESULTS

Equations (1) and (2) and the front equations derived in Paper I were integrated for different values of μ . In the following examples, the Lorentz factors of the fluids ahead and behind the front and the rest-frame Alfvén 4-velocity have been chosen to be, respectively, 5, 20, and 10. The magnetic pressure has been taken to decline as r^{-p} , and the intensity of background radiation as $f(r)/r^2$. A rapid magnetic field dissipation inside the front with the same decay constant as in the previous papers has been invoked. As a check, we computed the angular distribution of observed flux for a front with roughly time independent Lorentz factor (low radiative efficiency case), and compared the results with the analytic expressions, $\mathcal{F} \propto \mathcal{D}^\delta$, with $\delta = 3 + \alpha$ and $\delta = 4 + 2\alpha$ for synchrotron and ERC emission, respectively (Dermer 1995). The analytic results were reproduced to a very good accuracy by the numerical model.

Fig. 2 depicts the time profile of the front Lorentz factor, Γ_c , obtained for sufficiently long outbursts, in the sense that the shock travel time across the fluid slab is longer than the time change associated with the radial variations of magnetic field and ambient radiation intensity (see Paper I for more details). The radial profiles of magnetic field

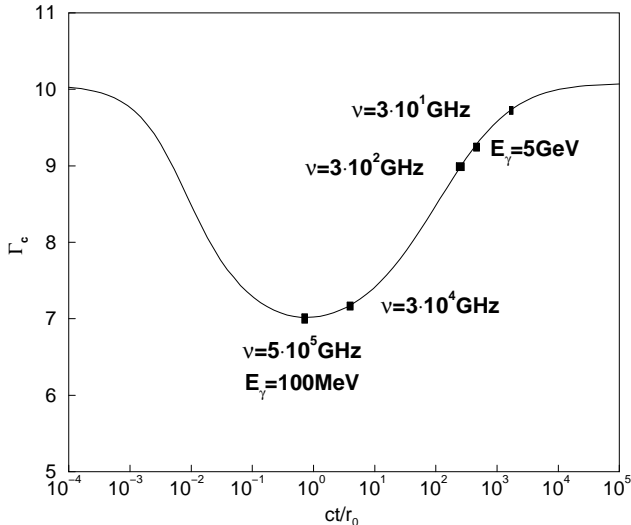


Figure 2. Time profile of the front Lorentz factor obtained for sufficiently long outbursts (see text). The times of peak emission at different energies are indicated

and external radiation field in this example are r^{-2} ($p = 2$, $f(r) = 1$). A steeper profile of the ambient radiation intensity leads quite generally to a larger acceleration of the front following peak emission, owing to the faster decrement of the radiative friction experienced by the front. The times of peak emission at different bands, and the corresponding Lorentz factors are indicated in the figure, and it is seen that the emission at different energies has different Doppler factors. This is essentially a consequence of the combination of dynamical and opacity effects. In addition to this dependence of Doppler factor on wavelength, there will also be a difference in the beaming patterns of synchrotron and ERC emission, owing to the difference in angular dependence of the corresponding volume emissivities (see below).

The resultant beaming patterns at different energies are delineated in fig. 3, where the relative dependences of the peak fluxes (normalized to their values at $\mu = 1$) on viewing angle are exhibited. The two gamma-ray bands shown correspond to the total gamma-ray flux above and below the threshold energy at which the pair production opacity (at $r = r_o$) is roughly unity. The difference in beaming patterns between synchrotron and ERC emission is clearly seen. Also evident is the stronger dependence of the optically thick emission on viewing angle. Although a model for the quiescent emission is required in order to calculate the amplitude of variations, the dependence of observed flux on μ shown in fig. 3 suggests that objects oriented to the observer at relatively large viewing angles may have preferentially larger amplitude outbursts at short wavelengths (optical/UV), and for small enough viewing angles also at gamma-ray energies below the break of the gamma-ray spectrum. It is also conceivable that intense outbursts at these energies will be followed by no activity at all at low frequencies.

The angular dependence of observed flux reflects, in this model, also the radial profiles of magnetic field and ambient radiation intensity. This is because both, the opacity and the front dynamics depend on the radial decrement of these quantities. Quite generally we find that the dependence of

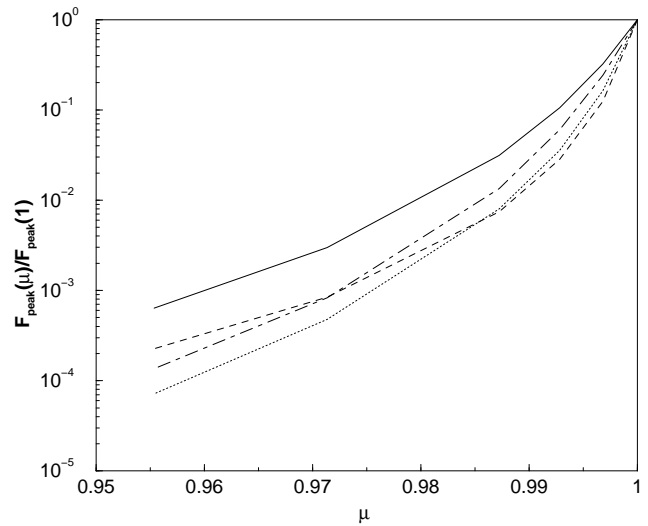


Figure 3. Peak fluxes (normalized to their values at $\mu = 1$) versus cosine of the viewing angle, at different energy bands: 5×10^5 GHz (with a logarithmic energy interval) (solid line), 3×10^2 GHz (dashed line), total gamma-ray flux in the energy interval 10 MeV to 1 GeV (dotted-dashed line), and 1 to 10 GeV (dotted line). An ambient radiation intensity profile with $f(r) = 1$ (corresponding to a r^{-2} profile) was used in this calculation

the ratio of optically thin and optically thick synchrotron fluxes on viewing angle becomes stronger for steeper ambient intensity profiles. The results obtained for ambient radiation intensity with an exponential profile, $f(r) = \exp(-r/r_1)$ (with $r_1 = 10r_o$ in this example), that may reflect the density profile of the surrounding gas that re-processes or scatters the nuclear radiation across the front, are shown in Fig. 4. As seen, the dependence of the optically thin fluxes on viewing angle is insensitive to the form of $f(r)$. However, the peak of the optically thick synchrotron flux declines more steeply with increasing viewing angle. This is because the front re-accelerates much faster in this case, owing to the rapid drop in radiative drag, so that the Doppler factor of the optically thick bands changes more rapidly. The behavior of optically thick ERC emission is more complicated; steeper ambient intensity profiles render the pair production opacity ahead of the front smaller which, in turn, leads to earlier ERC emission. This counteracts the effect associated with the faster acceleration and, therefore, the angular dependence of this component is more sensitive to the choice of parameters. In fact, in the example shown in Fig. 4 the decline of the total gamma-ray flux above the threshold energy to pair production at r_o is slower in the case of ambient intensity with an exponential profile, in contrast to the behavior of the low-frequency synchrotron emission.

The radial profile of the magnetic field affect mainly the synchrotron flux. Steeper profiles give rise to shorter delays of the low-frequency emission and, depending on the front acceleration scale, lead to a weaker dependence of the peak flux on viewing angle.

Fig. 5 presents sample light curves at various energies, computed for different viewing angles. As seen, for optically thick bands the shape of the light curve depends on μ , tending towards a much steeper decline at larger values of μ , thereby leading to a light curve that appears more symmet-

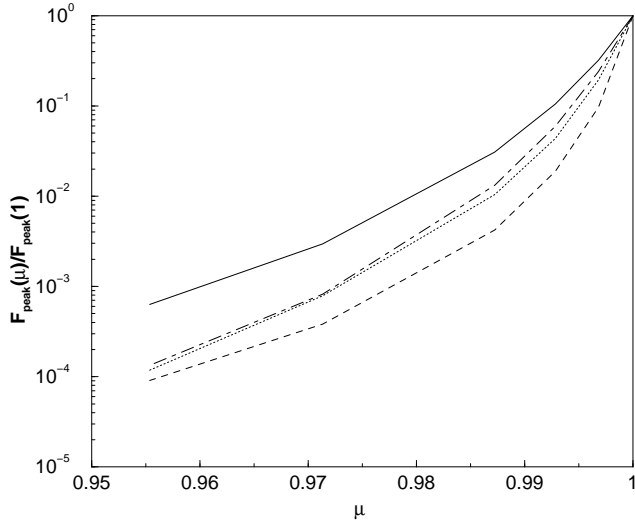


Figure 4. Same as fig. 3 but for $f(r) = \exp(-r/r_1)$, with $r_1 = 10r_o$

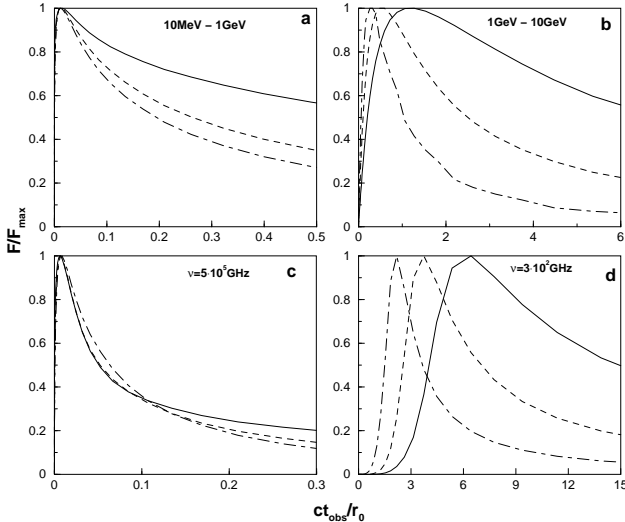


Figure 5. Sample light curves produced by the model, for $\mu = 1$ (solid line), $\mu = 0.99$ (dashed line), and $\mu = 0.97$ (dotted-dashed line). Each window corresponds to a given energy band (as indicated)

ric. Moreover, the time of peak emission and flare duration decrease with increasing viewing angle, as can be seen from the figure. This is again due to the evolution of the Doppler factor caused by the re-acceleration of the front. The optically thin bands show little dependence of flux decay time on viewing angle, as expected. We note that in situations where the ejected slabs are thin enough, or the ambient intensity has a much steeper radial profile, the flares will also tend to have a roughly symmetric shape.

In the case of sufficiently short outbursts, shock crossing is completed before front re-acceleration sets in. The dependence of the variability pattern on viewing angle would then be different than for long outbursts, and may depend on the cooling time of emitting electrons in the heated fluid slab. If only the fast slab is short, the reverse shock will decay quickly while the forward shock will continue to propagate

outward, similar to a GRB blast wave. This may give rise to somewhat different characteristics of the low-frequency emission. If both slabs are thin, then a lack of activity at long wavelengths, and a lower energy cutoff at gamma-ray energies are expected (see Paper II for a detailed discussion). The temporal behavior will be further complicated in situations in which multiple fronts with small enough duty cycle are created. This can lead to blending of different flares (as often seen at radio wavelengths; e.g., Aller, et al. 1985; Valtaoja, et al. 1999) and, in the case of ejection of a thin slab, to a collision of the decelerating slab, following shock crossing, with a newly expelled one, and the ultimate formation of a new shock in the radiating slab. Such episodes are far more difficult to simulate. Nonetheless, rapid, large amplitude flares should reflect the features associated with a single front.

4 CONCLUSIONS

We have considered the angular dependence of the observed variability pattern produced by internal fronts propagating through an ambient radiation field. We have shown that, for sufficiently long outbursts, the combination of dynamical effects caused by the radiative drag and optical depth effects, gives rise to a strong dependence of the observed flare's properties on source orientation.

To be more concrete, the shape of the light curves of optically thick emission reflects, at sufficiently large viewing angles, the temporal evolution of the Doppler factor, and at small viewing angles the evolution of the radiated power density. As a consequence, the time of peak emission and flare duration decrease with increasing viewing angle. Moreover, the flare appears to be more symmetric at larger viewing angles. The time evolution of optically thin emission is insensitive to source orientation, since it originates when the front is near its minimum Lorentz factor.

The time evolution of the beaming factors also renders the characteristics of correlated emission sensitive to source orientation. Because the source is inhomogeneous, the fluxes at different energies originate from different locations along the course of the front and, therefore, have different beaming cones due to the varying Lorentz factor. As a result the ratio of peak fluxes of the low-frequency (self-absorbed) and high-frequency synchrotron emission decreases with increasing viewing angle. The beaming cone of ERC emission is narrower than that of the synchrotron emission, leading to a somewhat more sensitive dependence of the gamma-ray flux on viewing angle than the high-frequency synchrotron flux. One implication of the above results is that sources that are oriented at relatively large viewing angles to the observer may exhibit events whereby strong gamma-ray and/or IR-optical-UV flares are followed by little or no activity of the low frequency (radio-to-millimeter) flux.

Finally, we note that the neglect of SSC emission may not be justified at large viewing angles, even in cases where the total power radiated is dominated by ERC emission. This is because the beaming cone of ERC photons is narrower than that of SSC photons (Dermer 1995). Thus, it is conceivable that in some regime of parameter space, the origin of observed gamma-rays also depends on the orientation of the source with respect to the observer.

This research was supported by The Israeli Science Foundation.

REFERENCES

Aller, H.D., Aller, M.F., Latimer, G.E., & Hodge, P.E. 1985, *ApJS*, 59, 513
 Blandford, R.D., & Levinson, A., 1995, *ApJ*, 441, 79
 Dermer, C.D. 1995, *ApJ*, 446, L63
 Eichler, D. 1994, *ApJS*, 90, 877
 Fishman, G.J., & Meegan, C.A. 1995, *ARA&A*, 33, 415
 Levinson, A. 1998, *ApJ*, 507, 145 (Paper I)
 Levinson, A. 1999a, *ApJ*, 522, 93 (Paper II)
 Levinson, A. 1999b, *AS&S*, in press
 Levinson, A., & Van Putten M.V.P., 1997, *ApJ*, 488, 69
 Rees, M, 1978, *MNRAS*, 184, 61
 Rees, M. & Meszaros, P, 1994, *ApJ*, 430, L93
 Romanova, M.M., & Lovelace, R.V.E. 1997, *ApJ*, 475, 97
 Sari, R., & Piran, T. 1997, *MNRAS*, 287, 110
 Ulrich, M.H., Maraschi, L., & Urry, C.M. 1997, *ARA&A*, 35, 445
 Valtaoja, E., Lahteenmaki, A., Terasranta, H., & Lainela, M. 1999, *ApJS*, 120, 95
 Wagner, S. 1997, in *Relativistic Jets in AGNs*, eds. M. Ostrowski et al., (Krakow: Poligrafia ITS), 208